




# Maximum Lyapunov Exponent Based Nearest Neighbour Algorithm For Real-Time Transient Stability Assessment

Sayyeda Umbereen Bano , Mehrdad Ghandhari   
KTH Royal Institute of Technology  
Div. of Electric Power and Energy Systems  
Stockholm, Sweden  
sayyeda@kth.se, mehrdad@kth.se

Robert Eriksson   
Swedish National Grid  
System Development  
Sundbyberg, Sweden  
robert.eriksson@svk.se

**Abstract**—In power systems, ensuring transient stability is paramount to prevent unforeseen blackouts and power failures. Transient stability assessment is crucial for the early detection and mitigation of instabilities, providing a rapid response to severe fault situations. The concept of the maximum Lyapunov exponent facilitates fast predictions for transient stability assessment after severe disturbances. This paper introduces an efficient maximum Lyapunov exponent algorithm for online transient stability assessment, representing the primary contribution of this work. This approach uses the time series data from the rotor angles of generators or the phase angles of generator terminal buses. Case studies are conducted on the Nordic Power System, with simulations performed in DigSilent PowerFactory. This study contributes by offering insights into the performance and adaptability of the proposed algorithm.

**Index Terms**—Maximal Lyapunov Exponent, Nordic Power System, Time Domain Simulation, Transient Stability Assessment, Phasor Measurement Unit, Nearest Neighbor Algorithm

## NOMENCLATURE

$\delta_i$	Rotor angle of $i_{th}$ generator.
$\omega_i$	Speed of $i_{th}$ generator.
$\theta_i$	Phase angle of $i_{th}$ generator terminal bus.
$\Delta t$	Simulation time step.
$t_c$	Fault clearing time.
$t_{id}$	Time of identification for critical and non-critical generators.
$t_{assess}$	Transient stability assessment time based on MLE.
$\delta_{re}$	Relative rotor angle of selected generators.
$\theta_{re}$	Relative phase angle of selected generator terminal buses.
$X(t)$	Phase space reconstructed vector.
$x(t)$	Time series data.
$\alpha_{mp}$	The mean period of the time series data.
$\rho_r$	Average divergence rate.
$N_i(\epsilon)$	$\epsilon$ -neighborhoods for each point in the $X(t)$ .

## I. INTRODUCTION

HISTORICALLY, Transient Stability Assessment (TSA) has garnered considerable research interest. Over time, a variety of methodologies emerged to address its complexities, each with its distinct benefits and constraints. Time Domain Simulation (TDS) has been a predominant tool for TSA, providing an exhaustive view of power system dynamics. However, due to its significant computational requirements, TDS is less suited for real-time TSA applications. This limitation prompted the advent of alternative approaches, such as the Transient Energy Function (TEF) [1] and SIngle Machine Equivalent (SIME) [2]. While these approaches offer faster assessment, they may face challenges in precisely modeling the intricacies of expansive, complex power systems [3]. PMU data has gained traction among the scientific community, particularly for TSA applications. For instance, the work in [4] explores the employment of self-adaptive decision trees for dynamic security assessment, enabling online detection of critical system parameters. The study in [5] leverages PMU data to draw comparative analyses anchored on stored trajectory patterns, subsequently applying these findings to TSA. Meanwhile, [6] presents an approach anchored on Artificial Neural Networks (ANNs). The proponents of this method underscore its computational efficiency and heightened precision, though it might face challenges when confronted with uncertainties, evolving network configurations, or infrequent system occurrences. Also, [7] presents a machine learning-based method for transient stability assessment, utilizing Long and Short-Term Memory (LSTM) classifiers for time-adaptive analysis and a trust score for reliability.

As discussed earlier, the methodologies for TSA proposed may face challenges. A primary challenge is achieving rapid detection of transient instability without depending on offline simulations or power system models, especially when no training data is available and computational resources are limited. Ensuring model accuracy and swiftly determining transient stability assessment remains a formidable challenge.

Within the power systems domain, the exploration of the

Submitted to the 23rd Power Systems Computation Conference (PSCC 2024).

Maximal Lyapunov Exponent (MLE) for online TSA is gaining traction. MLE can be calculated through two methods, model-based and model-free. The model-based approach relies on a comprehensive understanding of the system’s dynamical model [8], and applying this method to large-scale power systems presents challenges for online TSA due to its complexity [9] - [11]. However, based on model-based approach, MLE can be calculated using time series data from selected system variables. Thus, this approach offers a simpler solution for real-time applications. The model-free approach is the main focus of this paper.

The series of work in the domain of MLE based model-free approach begins with the introduction of Lyapunov Characteristic Exponents (LCEs) computation by [12]. It culminates in the robust method developed by [13] - [14], significantly contributing to the understanding of system dynamics, despite challenges such as sensitivity to noise and extensive data requirements. Comprehensive discussions and demonstrations of this model-independent methodology for computing MLE can be found in [12] - [19]. Alongside the evolution of MLE computation, recent studies have leveraged this approach for online monitoring and stability assessment of power systems [20] - [23]. For instance, a model-free MLE approach for rotor angle stability estimation was employed in [24], utilizing PMU data for online learning of system parameters. This concept was further advanced in [25], where a model-free approach was proposed. However, early post-fault MLE calculations are error-prone as model-free methods require some trajectory growth beforehand. As in [25], there are some optimal parameters to be selected, and their selection often depends on offline data. Thus, the selection of these parameters may limit the adaptability of MLE’s online TSA and may hamper its real-time applications due to the need for continuous adjustments. Furthermore, a contribution to online rotor angle stability assessment was made in [26] using PMU data, refining the method with a recursive least-squares-based MLE estimation and some critical parameters. However, this proposed technique in [26] may cause delays in online TSA since MLE estimation begins only after having identified those critical parameters based on the consistent pattern identification of the generator’s rotor speed.

The efficiency and accuracy of various previously established techniques for real-time transient stability assessment has been presented in [27].

The aim of this paper is to apply an MLE-based nearest neighbor algorithm for TSA.

Previous research has not sufficiently explored the MLE-based nearest neighbor algorithm’s capability to assess the stability of large power systems. This gap in the literature, combined with the critical need for rapid and accurate TSA, underscores the importance of this research.

The main contributions of this paper are given in the following.

- Firstly, this work overcomes the existing challenges of previous TSA techniques, such as the model dependency,

offline simulation data and consistent pattern identification, while also reducing the time required for transient stability assessment. This is achieved by providing an analytical formulation of the nearest neighbor algorithm that is suitable for power systems. The proposed MLE method presented in this paper—a synthesis of concepts from [13] and [14]—enables the development of a fast MLE algorithm that relies solely on data, making it model-free.

- Moreover, this study demonstrates that the proposed MLE algorithm functions effectively either with the rotor angles of selected generators or the phase angles of selected generator terminal buses. The examined scenario focuses on the large Nordic Power System (NPS) [29], which shows distinct nonlinear reactions subsequent to major disturbances. The study outlines results from diverse disturbances and simulations conducted using DigSilent Power Factory 2022 [30].

The rest of the paper is organized as follows: Section II introduces the MLE framework, setting the theoretical groundwork. Section III thoroughly explores the application of the proposed MLE to power systems, detailing its methodology and delving into practical applications through case studies to demonstrate the algorithm’s utility and effectiveness. The paper concludes with a summary of findings in Section IV and outlines future directions in Section V, encapsulating the study’s contributions.

## II. MAXIMAL LYAPUNOV EXPONENT FRAMEWORK

The dynamics of a system may be represented by a set of differential equations as:

$$\frac{dx}{dt} = f(x) \quad (1)$$

where,  $x$ , an  $n_x$ -dimensional state vector, resides in the Euclidean space  $R^{n_x}$ . The solution to (1) can be expressed as:

$$x(t) = x(t_0) + \int_{t_0}^t f(x) dt \quad (2)$$

where  $x(t_0)$  indicates the system’s initial state at time  $t = t_0$ . The MLE provides insight into the dynamics of a trajectory in proximity to  $x(t)$ , illustrated in Fig. 1. With  $\Delta x(t_0)$  sufficiently small, the trajectory’s sensitivity based on its initial condition is:

$$\Delta x(t) = \Delta x(t_0) e^{\lambda t} \quad (3)$$

The exponential term  $e^{\lambda t}$  describes the difference vector’s temporal evolution. From (3), deduce [12]:

$$\lambda = \lim_{t \rightarrow \infty} \frac{1}{t} \ln \frac{\|\Delta x(t)\|}{\|\Delta x(t_0)\|} \quad (4)$$

The MLE, denoted by  $\lambda$ , is an average based on the initial and final difference vector norms, offering insights into trajectory dynamics. System stability is inferred from the MLE’s sign: negative and positive values correspond to stable and unstable systems, respectively [12].

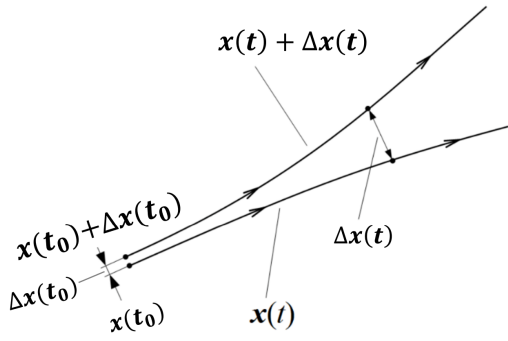


Fig. 1: Maximal Lyapunov Exponent Framework

### A. Model-Free Approach

In the model-free method, MLE is derived from time series data via phase space reconstruction [28]. This involves delay coordinate embedding, translating the series into a reconstructed domain. MLE, defined in (5), is evaluated by assessing distances between the main and nearby trajectories, emphasizing the logarithmic separation rate of adjacent points.

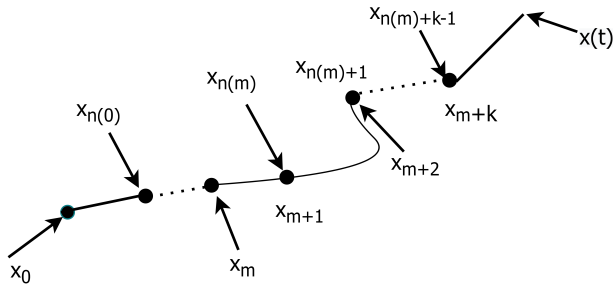


Fig. 2: Main and Nearby Trajectories in Model-Free Approach

As depicted in Fig. 2, both  $x_0$  and  $x_{n(0)}$  are the initial points on the original and neighboring trajectories, respectively. The term 'm' acts as an index, denoting the starting point for the MLE calculation within the time-series data. Additionally,  $x_{m+k}$  is the kth point after  $x_m$  on the original trajectory, and  $x_{n(m)+k}$  is the kth point after  $x_{n(m)}$  on the neighboring trajectory. Let  $|x_{n(m)} - x_m|$  be the Euclidean distance between the MLE estimation initial points, and  $|x_{n(m)+k} - x_{m+k}|$  be the Euclidean distance between the kth points after the MLE estimation initial point. As expressed in (5), MLE is then obtained as the average logarithmic rate of separation of nearest neighbor [15].

$$\lambda = \frac{1}{t_N} \sum_{k=1}^N \ln \left( \frac{|x_{n(m)+k} - x_{m+k}|}{|x_{n(m)} - x_m|} \right) \quad (5)$$

where  $t_N = N\Delta t$ , with  $\Delta t$  as the time step, and  $N$  as the total number of time steps.

### B. Formulation of Proposed MLE Approach

This approach aims to estimate the MLE by incorporating the  $\epsilon$ -neighborhood and scaling region concepts. The algorithm

fundamentally relies on the 'nearest neighbor' concept. This critical step of identifying the nearest neighbor ensures enhanced precision and robustness in the MLE estimation.

The discussions in this subsection largely follows those presented in [13] - [14].

The first step involves reconstructing the phase space attractor of the time series using the method of delays. The attractor is represented by a set of phase space vectors  $X(t)$ , which are constructed from the time series data as follows:

$$X(t) = [x(t), x(t+J), x(t+2J), \dots, x(t+(m-1)J)] \quad (6)$$

where,  $x(t)$  denotes the time series data,  $J$  represents the time delay, which is selected based on the methodology described in [14]. The parameter  $m$  stands for the embedding dimension. The next step is to define the  $\epsilon$ -neighborhoods for each point in the reconstructed phase space:

$$N_i(\epsilon) = \{j : \|X(i) - X(j)\| < \epsilon, i \neq j, |i-j| > \alpha_{mp}\} \quad (7)$$

For each pair of points within the  $\epsilon$ -neighborhoods, the initial and future distances are computed. These neighborhoods are sets of indices  $j$  where the Euclidean distance between points  $X(i)$  and  $X(j)$  is less than  $\epsilon$ . A constraint  $|i-j| > \alpha_{mp}$  from [13] is imposed to ensure that points within the same period are not considered, where  $\alpha_{mp}$  represents the mean period of the time series data. The initial distances between the points are computed as,

$$d_{ij}(0) = \|X(i) - X(j)\| \quad (8)$$

The future distances, after a time period  $t$ , are given by,

$$d_{ij}(t) = \|X(i+t) - X(j+t)\| \quad (9)$$

Figure 3 illustrates the process of identification of the closest neighbor to a given reference point.

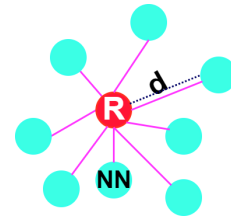


Fig. 3: Identifying Nearest Neighbor (NN) of Reference Point (R) in Trajectory via Minimum Distance (d)

The change in these distances over time helps to identify and understand the evolution and divergence of points in the phase space.

Next, the average divergence rate denoted by  $\rho_r$  is calculated at which the points within a neighborhood diverge from each other. It is computed as follows:

$$\rho_r = \frac{1}{|N_i(\epsilon)|} \cdot \sum_{j \in N_i(\epsilon)} \ln \frac{d_{ij}(t)}{d_{ij}(0)} \quad (10)$$

Where  $\epsilon$  defines the threshold for determining 'neighbors' of a reference point  $i$ . The set  $N_i(\epsilon)$  contains points within

a distance  $\epsilon$  from  $i$ . Once the average divergence rate is computed, the scaling region, denoted by  $\mathcal{S}$  is identified. The scaling region  $\mathcal{S}$  is the range of  $\epsilon$  values where there is a linear relationship between the logarithm of the initial and future distances. This can be achieved as follows:

1. For each  $\epsilon$  value, compute the logarithm of initial distances  $d_{ij}(0)$  and future distances  $d_{ij}(t)$ .
2. For each  $\epsilon$  value, fit a linear regression model of the form:

$$y(\epsilon) = a(\epsilon) \cdot \log d_{ij}(0) + b(\epsilon) \quad (11)$$

3. Calculate the coefficient of determination  $\mathcal{R}$  for each  $\epsilon$  value:

$$\mathcal{R}(\epsilon) = 1 - \frac{\sum (y(\epsilon) - \log d_{ij}(t))^2}{\sum (\log d_{ij}(t) - \mu_{d_{ij}(t)})^2} \quad (12)$$

In (12), the term  $\mu_{d_{ij}(t)}$  denotes the arithmetic mean of the logarithmic future distances  $\log d_{ij}(t)$ . These logarithmic future distances and their mean,  $\mu_{d_{ij}(t)}$ , are instrumental in determining  $\mathcal{S}$ . Specifically,  $\mathcal{S}$  is defined as the range of  $\epsilon$  values satisfying the condition,

$$\mathcal{R}(\epsilon) = \max_{\epsilon'} \mathcal{R}(\epsilon') \quad (13)$$

where  $\mathcal{R}$  measures the linear correlation between the logarithm of initial and future distances. A high  $\mathcal{R}$  value signifies a strong linear relationship, essential for the validity of this analysis. Therefore,  $\mathcal{S}$  represents the optimal region in the phase space for this investigation. Once the scaling region  $\mathcal{S}$  is identified, the process proceeds to estimate the largest Lyapunov exponent, denoted as  $\lambda$ . This is accomplished by averaging the divergence rates across all the neighborhoods within the scaling region as:

$$\lambda = \frac{1}{M} \cdot \sum_{i=1}^M \rho_{r_i} \quad (14)$$

where  $M$  represents the total number of neighborhoods within the scaling region. The largest Lyapunov exponent  $\lambda$  is an indicator of the average exponential rate of divergence or convergence of nearby orbits in phase space.



Fig. 4: Block Diagram of Proposed MLE Approach

If the MLE (i.e.  $\lambda$ ) is negative, the system is considered stable. Conversely, a positive MLE indicates an unstable system. This proposed method aims to provide accurate and robust estimates of the MLE. As a comprehensive overview, Fig. 4 provides a simplified representation of the proposed algorithm. It demonstrates the sequential process, starting from time series data acquisition, proceeding through phase space reconstruction and the nearest neighbor algorithm, and culminating with the computation of MLE via minimal distance. Each element in the diagram is clearly delineated: 'x' refer to (2), 'X' to (6), 'd<sub>ij</sub>' to (9), and 'λ' to (14).

### III. MLE APPLICATION TO POWER SYSTEMS

#### A. Selection of Time Series Data and MLE Calculation

The proposed MLE technique is implemented by collecting post-fault time series data of the rotor angles ( $\delta$ ) of the generator (or the phase angles ( $\theta$ ) of the generator terminal buses).

Consider now a system with  $n$  generators, and let  $x_i(t)$  be the time series data of the  $i^{\text{th}}$  generator (or terminal bus). Then for  $i = 1 \dots n$ ,  $x_i(t)$  is defined as:

$$\begin{aligned} x_i(t) &= \Delta\delta_i(t) = \delta_i(t) - \delta_i(t_0), \quad \text{or} \\ x_i(t) &= \Delta\theta_i(t) = \theta_i(t) - \theta_i(t_0) \end{aligned} \quad (15)$$

where,  $\delta_i(t_0)$  (or  $\theta_i(t_0)$ ) is the pre-fault value of the angle. Next, let  $t_c$  denote the fault clearing time, and  $t_{id} = t_c + t_\epsilon$  be the time at which the highest and lowest  $x(t_{id})$  are identified, respectively, as follows

$$\begin{aligned} x_k(t_{id}) &= \max(x_1(t_{id}), x_2(t_{id}), \dots, x_n(t_{id})), \\ x_l(t_{id}) &= \min(x_1(t_{id}), x_2(t_{id}), \dots, x_n(t_{id})). \end{aligned} \quad (16)$$

Having identified that the generator (or terminal bus)  $k$  has the highest  $x(t_{id})$ , and the generator (or terminal bus)  $l$  has the lowest  $x(t_{id})$  at  $t = t_{id}$ , then  $x_{re}(t)$ , is obtained by

$$x_{re}(t) = x_k(t) - x_l(t) \text{ for } t \geq t_{id} \quad (17)$$

where,  $x_{re}$  exemplifies the system metric equivalent to  $x$  in (5) and in this context,  $x_{re}(t_{id})$  corresponds to  $x_m$  in (5).

Let  $x_{re}(t)$  be either  $\delta_{re}(t)$  or  $\theta_{re}(t)$ ,  $\dot{x}_{re}(t) = \omega_{re}(t)$  and  $\ddot{x}_{re}(t) = \dot{\omega}_{re}(t)$  as illustrated in Fig 5. Let also  $t_{assess}$  be the time at which  $x_{re}(t)$  in the time interval  $t = [t_{id} \dots t_{assess}]$  (as  $x$  in Fig. 4) is used to assess the transient stability of a disturbance based on the sign of  $\lambda$  calculated in (14). The time  $t_{assess}$  is obtained based on the following steps.

- For  $t \geq t_{id}$ , compute  $x_{re}(t)$ ,  $\omega_{re}(t)$ ,  $S1 = \sin(x_{re})\omega_{re}$  and  $S2 = \dot{\omega}_{re}(t)$  as illustrated in Fig 5.
- Once the sign of one of the two signals  $S1$  and  $S2$  is firstly changed at time  $t = t_1$ , check the sign of  $\omega_{re}(t)$ ,
  - if  $\omega_{re}(t_1) > 0$ , set  $t_{assess} = t_1$  to calculate  $\lambda$  for TSA. A positive  $\lambda$  indicates a first swing instability.
  - if  $\omega_{re}(t_1) < 0$ , continue to compute  $x_{re}(t)$ ,  $\omega_{re}(t)$ , and the signal whose sign was firstly changed (i.e.  $S1$  or  $S2$ ) for  $t \geq t_1$ . Once the sign of that signal is changed again at time  $t = t_2$ , set  $t_{assess} = t_2$  to calculate  $\lambda$  for TSA.

These steps are illustrated in Fig. 6. As shown in the upper panel of the figure, at the time the signal  $S1$  passes the zero line (indicated by a red circle),  $\omega_{re}$  is positive (indicated by a black circle) and that time will be selected as  $t_{assess}$ . However in the bottom panel, once  $S1$  for the first time passes the zero line,  $\omega_{re}$  is negative. Therefore, the time at which the signal  $S1$  for the second time passes the zero line will be selected as  $t_{assess}$ .



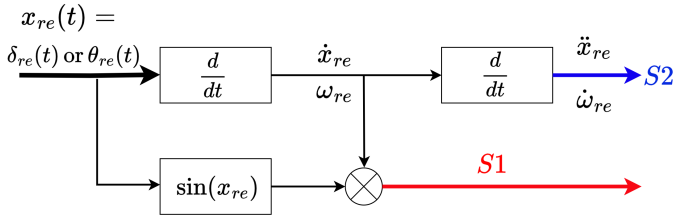


Fig. 5: Block Diagram of Stability Criterion. In this diagram, there are two signals:  $S1 = \sin(x_{re}) \omega_{re}$  and  $S2 = \dot{\omega}_{re}(t)$ , respectively.

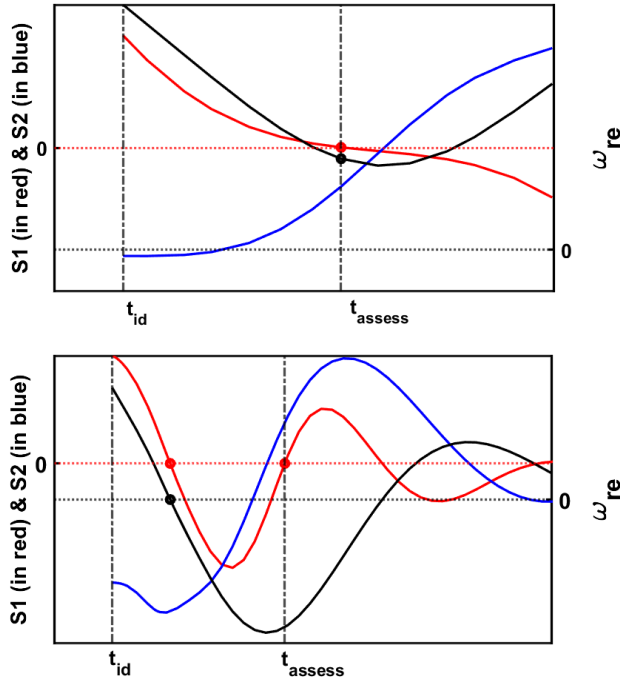


Fig. 6: Illustration of the discussed steps to obtain  $t_{assess}$ . Stable case in the upper panel and unstable case in the bottom panel.

### B. Test System

The proposed method is applied to the Northern European AC/DC power system, detailing the Nordic Power System (NPS) as described in [29]. In the test system (NPS), there are 16 generators in Norway (NO), 9 generators in Sweden (SE), 5 generators in Finland (FI), 29 generators in eastern Denmark (DK2), and 17 generators in western Denmark (DK1), respectively. DK1 synchronizes with Continental Europe (CE). The North Sea Wind Power Hub (NSWPH), Greater Britain (GB), and Continental Europe (CE) are represented using their Thévenin equivalent models.

All components within the system are represented by generic models, with the model being publicly available at [29], suitable for DigSilent PowerFactory 2022 or later versions. The single-line diagram of the NPS is depicted in a simplified form in Fig. 8, with the diagram predominantly featuring representations of Finland, Sweden, and Norway,

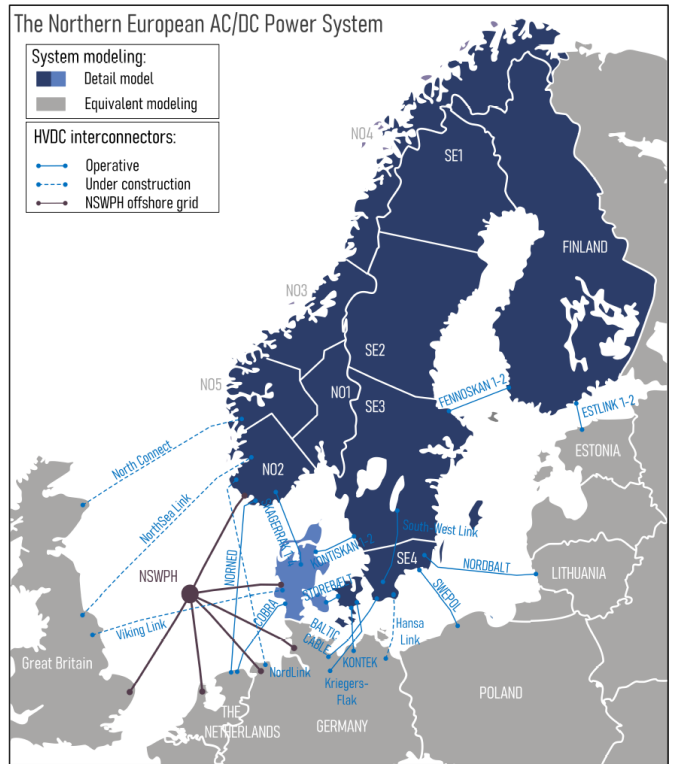


Fig. 7: Model of Northern Europe with North Sea Wind Power Hub, HVDC interconnectors (shown in blue), and the Nordic Power System (NPS) (in dark blue).

aligning with the study's focus on the NPS. A legend included in this figure elucidates the essential elements used in the diagram. In this depiction, entities like the North Sea Wind Power Hub (NSWPH), Eastern Denmark (DK2), Western Denmark (DK1), Greater Britain (GB), and Continental Europe (CE) are represented using their block models.

The principal portion of power originates from plants located along the Norwegian Coast and in Northern Sweden (NO3, NO4, NO5, SE1, and SE2 zones in Fig. 7). This energy is subsequently routed along a North-South axis to accommodate high demand in densely populated regions (NO1, NO2, SE3, SE4, and FI zones in Fig. 7).

### C. Case Studies

For application of MLE based TSA, 60 three-phase fault cases are implemented in the Nordic Power System as depicted in Fig. 8. These cases include both when only a fault is cleared and also when a fault is cleared by disconnecting a faulty line. Figure 9 shows the variations of the rotor angles deviations for an unstable case and a stable case, respectively.

In the application of the proposed MLE method, as detailed in Section III-A, at time  $t_{id} = t_c + t_e$ , the critical and non-critical generators are identified to establish  $\delta_{re}$  (or  $\theta_{re}$ ) as expressed in (17). In all cases,  $t_e$  corresponds to three simulation time steps which is about  $t_e = 0.04$  s. Then, the MLE based assessment is performed in the time interval  $t = [t_{id} \dots t_{assess}]$ , where  $t_{assess}$  is obtained based on the

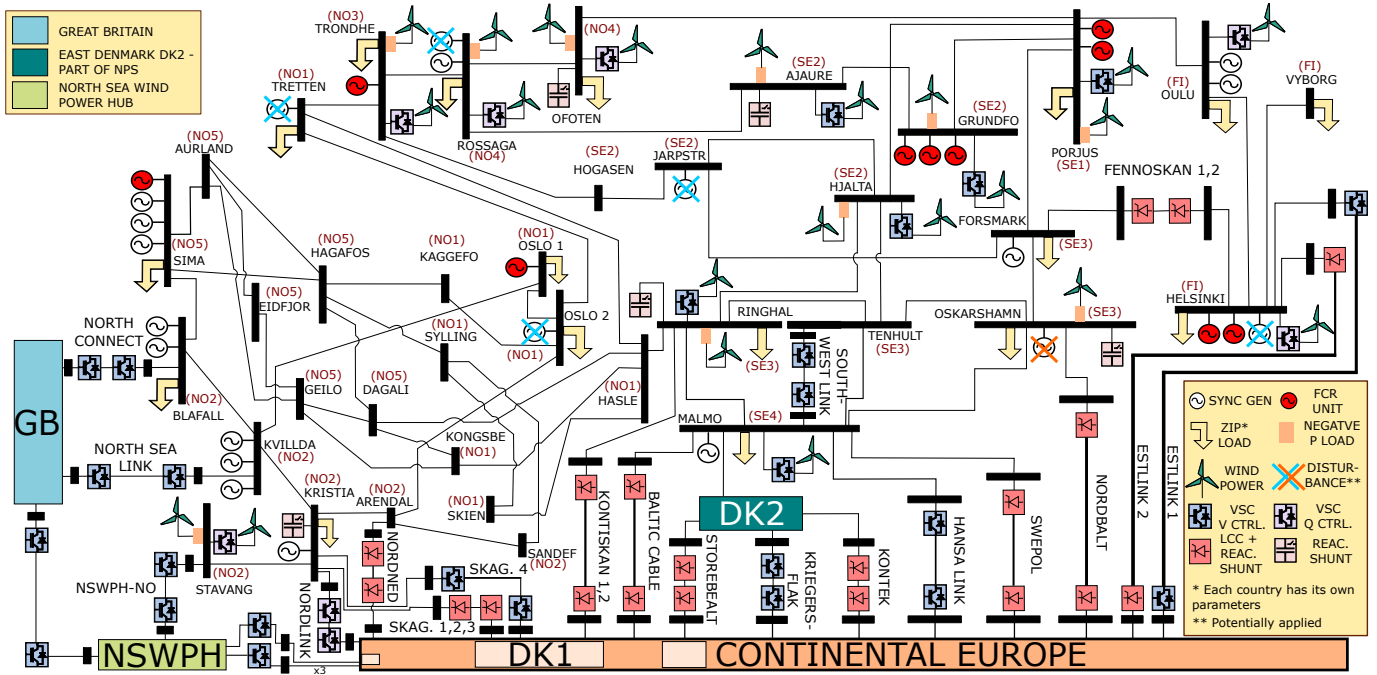


Fig. 8: Single line diagram of the Nordic Power System (NPS)

steps illustrated in Fig. 6. Thus, the total time duration for this assessment after the clearing time is  $\Delta t_{\text{assess}} = (t_{\text{assess}} - t_c)$ .

Comprehensive analysis of the proposed MLE behavior, indicative of stability and instability in the NPS system, is depicted in Fig. 10, featuring 60 MLE assessments of  $x_{re}(t) = \delta_{re}(t)$  following various fault cases.

In Fig. 10, the blue dots represent the initial values of MLE assessment at  $t_{id}$  and the blue circles represent the final values of MLE assessment at  $t_{\text{assess}}$ . The assessment points have positive values for unstable cases and negative values for stable cases. As shown in the figure, all MLE values based on  $\delta_{re}$  are negative for those 60 stable cases, and positive for the 60 unstable cases. This collective visualization of MLE curves underscores the method's consistent accuracy in TSA.

The longest assessment time  $\Delta t_{\text{assess}}$  for stable cases with  $\delta_{re}$  is 1.29 s, and the average  $\Delta t_{\text{assess}}$  for these cases is 0.64 s. Similarly, the longest assessment time  $\Delta t_{\text{assess}}$  for stable cases with  $\theta_{re}$  is 1.32 s, and the average  $\Delta t_{\text{assess}}$  for these cases is 0.55 s. The assessment time  $\Delta t_{\text{assess}}$  for stable cases are detailed in Table I.

For the majority of the stable cases based on  $\delta_{re}$ ,  $\Delta t_{\text{assess}} < 0.5$  s. A significant number of cases fall within the range  $0.5 \leq \Delta t_{\text{assess}} < 1$  s, and 12 out of 60 cases have the longest assessment times within  $1 \leq \Delta t_{\text{assess}} < 1.3$  s.

Similarly, for the majority of the stable cases based on  $\theta_{re}$ ,  $\Delta t_{\text{assess}} < 0.5$  s, with a large number of cases also in the range  $0.5 \leq \Delta t_{\text{assess}} < 1$  s, and 3 out of 60 cases have the longest assessment times within  $1 \leq \Delta t_{\text{assess}} < 1.3$  s. The emergence of assessment time  $\Delta t_{\text{assess}}$  clusters around  $\Delta t_{\text{assess}} < 1$  (s) may reflect groups of cases with similar TSA challenges.

The longest assessment time  $\Delta t_{\text{assess}}$  for unstable cases with

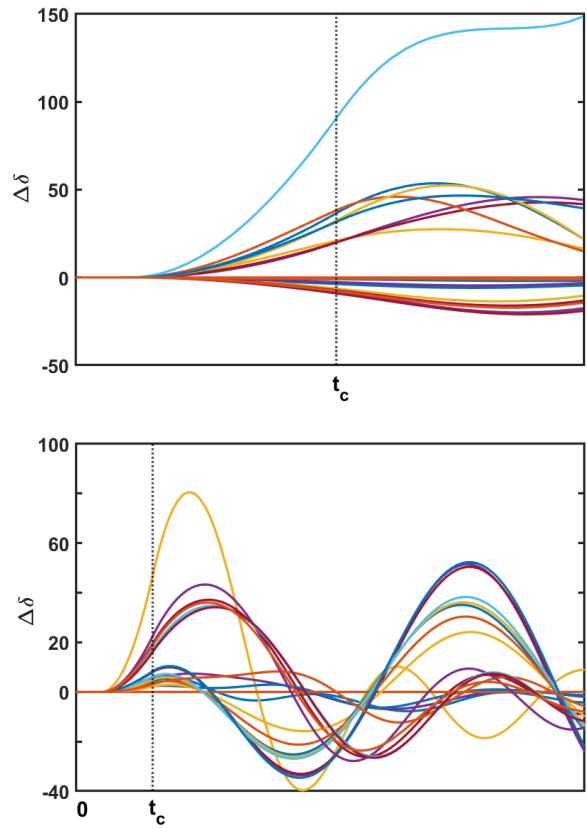


Fig. 9: Variations of rotor angles deviations for an unstable case (upper panel) and a stable case (bottom panel), respectively.

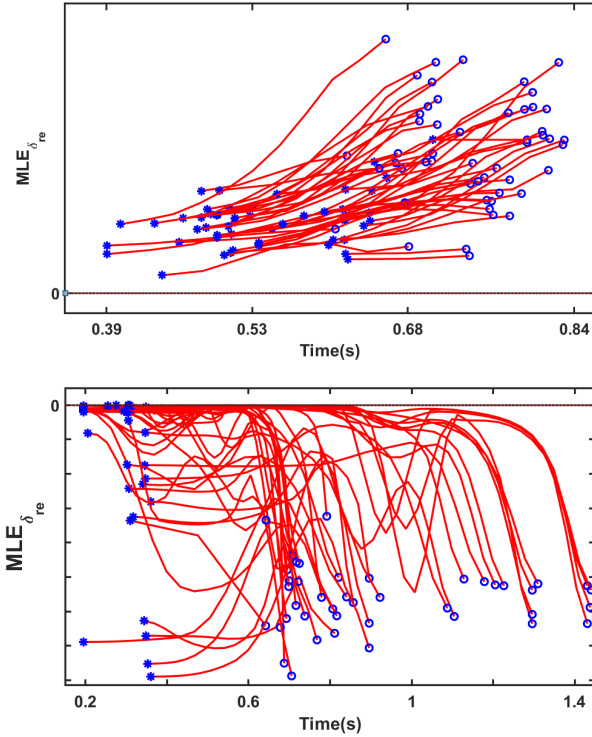


Fig. 10: The collective visualization of MLE curves highlights MLE's consistent predictive of transient instability in the upper figure, and transient stability in the lower figure, respectively.

TABLE I: Summary of TSA Results for Stable Cases

Range of $\Delta t_{\text{assess}}$	No. of Cases ( $\delta_{re}$ )	No. of Cases ( $\theta_{re}$ )
$\Delta t_{\text{assess}} < 0.5$ s	27	24
$0.5 \leq \Delta t_{\text{assess}} < 1$ s	21	41
$1 \leq \Delta t_{\text{assess}} < 1.3$ s	12	3

$\delta_{re}$  is 0.36 s, and the average  $\Delta t_{\text{assess}}$  for these cases is 0.22 s. Similarly, the longest assessment time  $\Delta t_{\text{assess}}$  for unstable cases with  $\theta_{re}$  is 0.41 s, and the average  $\Delta t_{\text{assess}}$  for these cases is 0.20 s. The assessment time  $\Delta t_{\text{assess}}$  for stable cases are detailed in Table II.

#### IV. CONCLUSION

The nearest neighbor based Maximum Lyapunov Exponent (MLE) algorithm has been adapted for power systems, demonstrating success in transient stability assessment across all 60 stable and unstable fault cases for both  $\delta_{re}(t)$  and  $\theta_{re}(t)$ . A criterion based on two signals S1 and S2 has been developed to quickly identify potential first swing instabilities. For the stable cases, the longest assessment times  $\Delta t_{\text{assess}}$  were 1.29 s with  $\delta_{re}$  and 1.32 s with  $\theta_{re}$ , and the average assessment times  $\Delta t_{\text{assess}}$  were 0.64 s with  $\delta_{re}$  and 0.55 s with  $\theta_{re}$ , respectively. For the unstable cases, the longest assessment times  $\Delta t_{\text{assess}}$  were 0.36 s with  $\delta_{re}$  and 0.41 s with  $\theta_{re}$ , and the average assessment times  $\Delta t_{\text{assess}}$  were 0.22 s with  $\delta_{re}$  and 0.20 s with  $\theta_{re}$ , respectively. The accuracy of these results underscores the

TABLE II: Summary of TSA Results for Unstable Cases

Range of $\Delta t_{\text{assess}}$	No. of Cases ( $\delta_{re}$ )	No. of Cases ( $\theta_{re}$ )
$\Delta t_{\text{assess}} < 0.2$ s	22	26
$0.2 \leq \Delta t_{\text{assess}} < 0.3$ s	32	31
$0.3 \leq \Delta t_{\text{assess}} < 0.4$ s	6	3

algorithm's effectiveness for online TSA, marking a significant advancement in detecting transient instabilities by operating independently of preset offline values and relying entirely on real-time data.

Further research concluded that the phase angles of selected generator terminal buses can effectively replace the rotor angles of selected generators.

#### V. FUTURE WORK

Future research should evaluate the application of this method using real PMU data and its integration with corrective actions, such as the connection of braking resistors, fast valving, and control of power electronic based devices, to enhance transient stability. Furthermore, optimizing the nearest neighbor MLE algorithm and also identifying additional criteria will be necessary to improve TSA assessment, by reducing the assessment time  $\Delta t_{\text{assess}}$ , thereby enhancing its practicality for online applications.

#### REFERENCES

- [1] M. A. Pai, Energy Function Analysis for Power System Stability, Kluwer Academic Publishers, 1989.
- [2] M. Pavella, D. Ernst and D. Ruiz-Vega Power System Transient Stability Analysis and Control, Kluwer Academic Publishers, 2000.
- [3] J. H. Chow, A. Chakraborty, M. Arcak, B. Bhargava, and A. Salazar, "Synchronized phasor data-based energy function analysis of dominant power transfer paths in large power systems," IEEE Trans. Power Syst., vol. 22, no. 2, pp. 727–734, May 2007.
- [4] K. Sun et al., "An online dynamic security assessment scheme using phasor measurements and decision trees," IEEE Trans. Power Syst., vol.22, no. 4, pp. 1935–1943, Nov. 2007.
- [5] C. W. Liu and J. S. Thorp, "New methods for computing power system dynamic response for online transient stability prediction," IEEE Trans. Circuits Syst. I, Fundam. Theory Appl., vol. 47, no. 3, pp. 324–337, Mar. 2000.
- [6] C.W. Liu, M.Ch. Su, S.-S. Tsay, Y.J. Wang, "Application of a novel fuzzy neural network to online transient stability swings prediction based on synchronized phasor measurements," in IEEE Trans. Power Syst., 14 (1999), pp. 685-692.
- [7] Huaiyuan Wang, Sijie Wu, "Transient stability assessment with time-adaptive method based on spatial distribution," in International Journal of Electrical Power & Energy Systems, Volume 143,2022, 108464, ISSN 0142-0615, doi: 10.1016/j.ijepes.2022.108464.
- [8] J. Hu, T. Wang, Z. Wang, J. Liu and J. Bi, "Switching System's MLE Based Transient Stability Assessment of AC/DC Hybrid System Considering Continuous Commutation Failure," in IEEE Transactions on Power Systems, vol. 36, no. 1, pp. 757-768, Jan. 2021, doi: 10.1109/TPWRS.2020.3007651.
- [9] C. Skokos, G. A. Gottwald, and J. Laskar, Chaos Detection and Predictability. Heidelberg, Germany: Springer, 2016
- [10] C.W. Liu et al., "Detection of transiently chaotic swings in power systems using real-time phasor measurements," IEEE Trans. Power Syst., vol. 9, no. 3, pp. 1285–1292, Aug. 1994.
- [11] J. Yan, C. Liu, and U. Vaidya, "PMU-based monitoring of rotor angle dynamics," IEEE Trans. Power Syst., vol. 26, pp. 2125–2133, 2011.

- [12] Benettin, Giancarlo, Galgani, L. Giorgilli, Antonio Strelcyn, Jean-Marie. (1980). Lyapunov characteristic exponents for smooth dynamical systems and for Hamiltonian systems - A method for computing all of them. I - Theory. II - Numerical application. *Meccanica*. 15. 21-30. 10.1007/BF02128236.
- [13] M. T. Rosenstein, J. J. Collins, and C. J. De Luca, "A practical method for calculating largest Lyapunov exponents from small data sets," *Phys.D*, vol. 65, nos. 1/2, pp. 117–134, May 1993.
- [14] H. Kantz, "A robust method to estimate the maximal Lyapunov exponent of a time series," *Phys. Lett. A*, vol. 185, no. 1, pp. 77–87, Jan. 1994.
- [15] M. Sano and Y. Sawada, Measurement of the Lyapunov spectrum from a chaotic time series, *Phys. Rev. Lett.* 55 (1985) 1082.
- [16] Eckmann, Jean-Pierre Ruelle, D. (1985). Ruelle, D.: Ergodic theory of chaos.
- [17] P. Bryant, R. Brown, and H. Abarbanel, "Lyapunov exponents from observed time series," *Phys. Rev. Lett.*, vol. 65, no. 13, pp. 1523–1526, Sep. 1990.
- [18] K. Geist, U. Parlitz, and W. Lauterborn, "Comparison of different methods for computing Lyapunov exponents," *Prog. Theor. Phys.*, vol. 83, pp. 875–893, May 1990.
- [19] X. Zeng, R. Eykholt and R.A. Pielke, "Estimating the Lyapunov-exponent spectrum from short time series of low precision," *Phys. Rev. Lett.*, vol. 66, pp. 3229–3232, 1991.
- [20] C.W. Liu et al., "Detection of transiently chaotic swings in power systems using online phasor measurements," *IEEE Trans. Power Syst.*, vol. 9, no. 3, pp. 1285–1292, Aug. 1994.
- [21] X. D. Liu, Y. Li, Z. J. Liu, Z. G. Huang, Y. Q. Miao, Q. Jun, Q. Y. Jiang, and W. H. Chen, "A Novel Fast Transient Stability Prediction Method Based on PMU," 2009 Power & Energy Society General Meeting, Calgary, Alberta Canada, July. 26-30 2009.
- [22] J. Yan, C. Liu, and U. Vaidya, "PMU-based monitoring of rotor angle dynamics," *IEEE Trans. Power Syst.*, vol. 26, pp. 2125–2133, 2011.
- [23] S. Dasgupta, M. Paramasivam, U. Vaidya, and V. Ajjrapu, "online monitoring of short-term voltage stability using PMU data," *IEEE Trans. Power Syst.*, vol. 28, no. 4, pp. 3702–3711, Nov. 2013.
- [24] S. Dasgupta, M. Paramasivam, U. Vaidya and V. Ajjrapu, "PMU-Based Model-Free Approach for online Rotor Angle Monitoring," in *IEEE Transactions on Power Systems*, vol. 30, no. 5, pp. 2818–2819, Sept. 2015.
- [25] Huang, Dan, Chen, Qiyu, Ma, Shiyong, Zhang, Yichi and Chen, Shuyong, (2018), Wide-Area Measurement—Based Model-Free Approach for Online Power System Transient Stability Assessment, *Energies*, 11, issue 4, p. 1-20.
- [26] S. Wei, M. Yang, J. Qi, J. Wang, S. Ma and X. Han, "Model-Free MLE Estimation for Online Rotor Angle Stability Assessment With PMU Data," in *IEEE Transactions on Power Systems*, vol. 33, no. 3, pp. 2463–2476, May 2018.
- [27] Sayyeda Umbereen Bano, Mehrdad Ghandhari, Robert Eriksson, "A Comparative Analysis Of Techniques For online Transient Stability Assessment," 2022 54th North American Power Symposium, 2022.
- [28] A. Wolf, J. B. Swift, H. L. Swinney, and J. A. Vastano, "Determining Lyapunov exponents from a time series," *Phys. D*, vol. 16, no. 3, pp. 285–317, Jul. 1985.
- [29] D. Obradović, M. Dijokas, G. S. Misyris, T. Weckesser and T. Van Cutsem, "Frequency Dynamics of the Northern European AC/DC Power System: A Look-Ahead Study," in *IEEE Transactions on Power Systems*, vol. 37, no. 6, pp. 4661–4672, Nov. 2022, doi: 10.1109/TPWRS.2022.3154720.
- [30] "Powerfactory 2022: User Manual," DIgSILENT GmbH, Gomaringen, Germany, June, 2022.